MODELLING AND SIMULATION OF LEAN HYDROGEN-AIR DEFLAGRATIONS IN 120 M^3 ENCLOSURE

Makarov, D., Molkov, V.
Hydrogen Safety Engineering and Research Centre (HySAFER),
University of Ulster, Shore Road, Newtownabbey, BT37 0QB, UK, dv.makarov@ulster.ac.uk

ABSTRACT

The paper describes CFD modelling of lean hydrogen mixture deflagrations. Large eddy simulation (LES) premixed combustion model developed at the University of Ulster to account phenomena related to large-scale deflagrations was adjusted specifically for lean hydrogen-air flames. Experiments by Kumar (2006) on lean hydrogen-air mixture deflagrations in a 120 m^3 vessel at initially quiescent conditions were simulated. 10% by volume hydrogen-air mixture was chosen for simulation to provide stable downward flame propagation; experiments with the smallest vent area 0.55 m^2 were used as having the least apparent flame instabilities affecting the pressure dynamics. Deflagrations with igniter located centrally, near vent and at far from the vent wall were simulated. Analysis of simulation results and experimental pressure dynamics demonstrated that flame instabilities developing after vent opening made the significant contribution to maximum overpressure in the considered experiments. Potential causes of flame instabilities are discussed and their comparative role for different igniter locations is demonstrated.

1.0 INTRODUCTION

Safe indoor use of hydrogen and fuel cell systems requires closing knowledge gaps in prediction, assessment and mitigation of hazards, particularly those associated with deflagrations of lean hydrogen-air mixtures. Hydrogen releases from hydrogen installations or infrastructure cannot be completely avoided. Should this occur in a large-scale facility, the credible release scenario leads to formation of a lean hydrogen-air mixture rather than a near-stoichiometric one. Yet, modelling of turbulent premixed combustion of lean hydrogen-air mixtures using methods of Computational Fluid Dynamics (CFD) remains a challenging task, predictive capabilities of practical modelling tools in this area remains uncertain, and high-quality well documented experiments for validation are few and scattered.

Turbulent combustion of lean hydrogen-air mixtures is difficult to model and then simulate with satisfactory predictive capability. This is caused by lack or uncertainty of experimental data on lean hydrogen-air mixture properties, and lack of physical understanding and models to address the specific phenomena at large scales which may include interaction of a number of istabilities: thermo-diffusive instability, hydrodynamics instability developing at large scales, high sensitivity of flame propagation behaviour to hydrogen concentration when approaching the lower flammability limit, etc.

The present paper describes a preliminary attempt to model lean hydrogen-air mixture deflagrations using the large eddy simulation (LES) multi-phenomena deflagration model, which is being developed at the University of Ulster [1]. The study aims at testing predictive capabilities of the current model for lean hydrogen mixture deflagrations at large scales, as well as understanding and quantifying impact of not yet accounted for in the multi-phenomena turbulent burning velocity model of deflagration [1] mechanisms of combustion acceleration and flame instabilities on pressure dynamics and maximum pressure loads.

Impact of flame instabilities and oscillatory combustion-acoustic interaction, expected to be particularly pronounced for lean hydrogen mixture deflagrations, was studied back in 1980-es based on hydrocarbon mixture deflagrations, e.g. see Van Wingerden and Zeeuwen [2], and Cooper et al. [3]. Van Wingerden and Zeeuwen noted that sensitivity to the pressure waves and ability to pressure-acoustic coupling is property of the gas mixtures exhibiting “spontaneous cell structure” (i.e. thermo-

diffusively unstable). It appears that acoustic instability affects the final stage of combustion in enclosure: Van Wingerden and Zeeuwen stated that the final pressure peak was "invariably accompanied by pressure fluctuations … caused by a standing acoustic wave". Cooper et al. claimed that the pressure peak is generated when pressure waves couple with acoustic modes of the vessel giving rise to high combustion rates. The phenomenon occurred when combustion was confined to isolated pockets in the vessel corners [3]. Another analysis of combustion instabilities during vented deflagrations was performed by Solberg and co-workers [4] based on their experiments in 35 m^3 vessel. They observed that in a rear ignition case the sudden change of flow velocity in a vent (at the moment when the combustion products venting starts) causes large-scale turbulence and flame instabilities in enclosure, leading to a strong combustion acceleration and a pressure peak. A strong pressure peak for the central ignition, on the other hand, was "very likely … due to a Taylor instability" developing at the rear part of the flame. Solberg concluded that Taylor instability, developing from the moment of venting, may be the dominating mechanism governing the pressure load from vented explosions. Solberg and co-workers also acknowledged the effect of combustion-acoustic coupling observing it using high-speed video records. They noted that the pressure peaks from flame instabilities and acoustic interaction appear to be less dominant in smaller-scale explosions. Layer and Manson [5] suggested that the amplification of acoustic instabilities in a small scale pipe occurs when the inducing pressure waves exceed value 5 kPa.

Importance of flame-acoustic interaction and instabilities for hydrogen-air mixtures was confirmed in the experimental programme by FM Global on ~18% vol. hydrogen-air mixture deflagrations conducted in a 64 m^3 vessel [6]. While first pressure peak in all experiments was associated with combustion products venting and external explosion, the authors associated the second peak (though not always dominant) with flame-acoustic interaction. The second peak was present in experiments with both central and rear wall ignition, and with two different vent areas 2.7 m^2 and 5.4 m^2.

2.0 EXPERIMENTAL DETAILS

Series of experiments on deflagrations of lean hydrogen-air mixtures in a range of hydrogen concentrations and vent sizes is described in [7]. The experiments were performed at Atomic Energy of Canada Ltd. The research programme was undertaken with specific aim to determine the effect of deflagration enclosure scale on combustion behaviour and ignitor location on peak overpressure [7].

The experimental facility was a rectangular enclosure constructed of 1.25 cm steel plates attached to I-beams bolted to 1-m thick concrete pad. The enclosure sizes were 10 m length, 4 m width, and 3 m height (total volume 120 m^3). The vent was located on the front wall and designed to be adjusted to areas 0.55, 1.09, and 2.19 m^2, in all cases the vent height was 0.74 m. The vent covers were made of aluminium foil with small tears to facilitate rapture at small overpressures. Three different ignition locations were used in experiments: 18 cm from the rear wall, in the middle of the enclosure, and 18 cm from the front wall with the vent, all on the centre-line across longest enclosure dimension. Ignition of the mixture was achieved by a glow plug, ignition occurred approximately 25 s after switching on the power. In the experimental report it was stressed that combustion mixture preparation was well controlled and the mixture composition error was within ±0.17% vol. The experimental programme included deflagrations with the three aforementioned ignition locations, all three vent areas, and hydrogen volume fraction ranging from 6% to 12% vol. All experiments are said to be conducted "at room temperature and near-atmospheric pressures" [7].

The experiment description [7] included not-filtered experimental pressure dynamics for some hydrogen mixtures and ignition locations, and analysis of peak overpressure variation as a function of hydrogen concentration and ignitor location. The peak pressures with front-wall (near-vent) ignition were generally found to be much smaller than those with the rear-wall (far-vent) and central ignition. With rear-wall ignition, the peak pressure increased with hydrogen volume fraction and reached local maximum at 9% vol. hydrogen; with further increase of hydrogen fraction it decreased and provided a local minimum at 10% vol.; above hydrogen fraction 10% vol. the peak pressure generated by the rear-wall ignition increased again.

Deflagration experiments with 10% vol. hydrogen mixture and 0.55 m^2 vent area were chosen for numerical simulation. Deflagrations with the smallest vent area produced the least pressure oscillations and may be expected to have the least pronounced combustion instabilities. Mixture outflow from the smallest vent will have the least potential for an external explosion. The experiments with 10% vol. hydrogen fraction were chosen to have stable and reliable flame propagation through the experimental enclosure for the LES deflagration model to be applicable (as downward flame propagation limit is 9% vol. hydrogen fraction [7]).

3.0 ULSTER LES DEFLAGRATION MODEL AND SIMULATION DETAILS

3.1 Outline of Ulster LES model

The LES deflagration model has being developed at the University of Ulster and based on the turbulent burning velocity combustion sub-model taking into account physical phenomena responsible for flame wrinkling and combustion acceleration at large scales. The model was extensively validated against deflagration experiments with stoichiometric and near-stoichiometric mixtures, e.g. validation against set of 22 experiments was undertaken in [8], comparison of the model and results with other simulation tools and results of their applications for selected hydrogen deflagration experiments may be found in [9-13]. The latest model description and references to validation studies may be found elsewhere [1] and only the main model features are given below to enable discussion of model adjustment for lean and buoyant mixtures combustion.

The progress variable equation (1) and the gradient method for mass burning rate (2) are in the core of the model to simulate flame front propagation and mass burning rate respectively:

$$\frac{\partial}{\partial t}\left(\overline{\rho}\,\widetilde{c}\right)+\frac{\partial}{\partial x_j}\left(\overline{\rho}\,\widetilde{u}_j\widetilde{c}\right)=\frac{\partial}{\partial x_j}\left(\frac{\mu_{eff}}{Sc_{eff}}\frac{\partial \widetilde{c}}{\partial x_j}\right)+\overline{S}_c\,, \tag{1}$$

$$\overline{S}_c=\rho_u S_t\left|grad\,\widetilde{c}\right|. \tag{2}$$

where ρ - density, u_j - velocity components, c - combustion progress variable, t - time, x_j - spatial coordinates, μ_{eff} – effective dynamic viscosity, Sc_{eff} – effective Schmidt number, S_c - source term in the progress variable equation, ρ_u – density of unburned mixture, S_t - turbulent burning velocity. The sub-grid scale (SGS) viscosity, Prandtle and Schmidt numbers are calculated based on renormalization group (RNG) model by Yakhot [14]. The sub-grid scale burning velocity S_t accounts flow turbulence in the incoming unburned mixture based on the turbulent premixed burning velocity model by Yakhot [15]. Dependence of laminar burning velocity S_u on hydrogen concentration is modelled based on experimental measurements [16], and dependence on transient pressure and temperature - according to [17]. The following additional flame wrinkling factors, leading to augmentation of mass burning rate and playing role at large scales, are incorporated in the combustion model to reflect phenomena:

- Ξ_K to account the flame front generated turbulence following the theory by Karlovitz et al. [18];
- Ξ_f to account fractal nature of flame surface for large-scale flames with fractals dimension as a function of sub-grid-scale velocity *u'* adopted following [19];
- Ξ_{lp} to account the preferential diffusion of stretched flames via the leading point concept [20].

The resultant equation for the sub-grid scale burning velocity is modelled using a modified form of Yakhot's equation for premixed turbulent burning velocity:

$$S_t=\left[S_u\left(Y_{H2},p,T\right)\cdot\Xi_K\cdot\Xi_{lp}\cdot\Xi_f\right]\cdot\exp\left(\frac{u'}{S_t}\right)^2, \tag{3}$$

where S_u - laminar burning velocity, Y_{H2} – hydrogen mass fraction, p – pressure, T – temperature, u' – SGS velocity. The product of flame wrinkling factors $\left(\Xi_K\cdot\Xi_{lp}\cdot\Xi_f\right)$ in the above equation describes

the unresolved flame wrinkling at sub-grid scales comparable with the flame thickness. The term $\left[S_u\left(Y_{H2}, p, T\right)\cdot\Xi_K\cdot\Xi_{lp}\cdot\Xi_f\right]$ is acting instead of the laminar burning velocity in the original Yakhot's equation [15].

3.2 LES model adaptation for lean hydrogen-air mixtures

3.2.1 Development of flame wrinkling with time

The described above model was developed for flames not affected by buoyancy, hence it was validated against mostly stoichiometric and nearly stoichiometric mixtures which flames are initially spherically propagating. As a matter of convenience, the development of flame wrinkling factors Ξ_K, Ξ_{lp}, Ξ_f was modelled as a function of flame radius R and the critical radius for the onset of fully turbulent regime of flame front propagation R_0:

$$\Xi_K = 1+\left(\psi\cdot\Xi_K^{\max}-1\right)\cdot\left[1-\exp\left(-\frac{R}{R_0}\right)\right], \tag{4}$$

$$\Xi_{lp} = MIN\left\{\Xi_{lp}^{\max};1+\frac{\left(\Xi_{lp}^{\max}-1\right)\cdot R}{R_{0_{lp}}}\right\}, \tag{5}$$

$$\Xi_f = MAX\left\{1;\left(\frac{R}{R_0}\cdot\frac{\varepsilon_{R_0}}{\varepsilon}\right)^{D-2}\right\}, \tag{6}$$

where $\Xi_K^{\max}$ - maximum flame wrinkling factor due to flame induced turbulence, $\Xi_{lp}^{\max}$ - maximum flame wrinkling according to the leading points concept, R – flame radius, R_0 – characteristic flame radius for onset of fully turbulent flame propagation regime, $R_{0_{lp}}$ - characteristic radius for complete development of flame wrinkling due to leading points, ε and ε_{R_0} - inner cut-off and inner cut-off at radius R_0 respectively, The upper limit of flame wrinkling factor due to self-induced turbulence in Eq.(4) can be calculated as $\Xi_K^{\max}=(E-1)/\sqrt{3}$ [1,21], the upper limit for the leading point flame wrinkling factor $\Xi_{lp}^{\max}$ is a function of hydrogen concentration adopted from [20], and the characteristic radius for transition to fully developed flame wrinkling due to leading point mechanism $R_{0_{lp}}$ is calculated as half of the characteristic radius R_0, i.e. $R_{0_{lp}}=R_0/2$, see e.g. [1].

To adopt the model for buoyant flames, where flame distance from ignition point is not a unique value for the whole flame surface, Karlovitz and leading point wrinkling factors were modelled as functions of time:

$$\Xi_K = 1+\left(\psi\cdot\Xi_K^{\max}-1\right)\cdot\left[1-\exp\left(-\frac{t}{t_0}\right)\right], \tag{7}$$

$$\Xi_{lp} = MIN\left\{\Xi_{lp}^{\max};1+\frac{\left(\Xi_{lp}^{\max}-1\right)\cdot t}{t_{0lp}}\right\}. \tag{8}$$

Here the characteristic times t_{0lp} and t_0 correspond to the moments when the flame would reach radii $R_{0_{lp}}$ and R_0 respectively if it were developing without effect of buoyancy in a spherical shape (i.e. as

though in microgravity). Characteristic times t_{0lp} and t_0 were found prior to CFD simulations from numerical integration of flame speed with time: $dR = E \cdot \left(S_u\left(Y_{H2}, p, T\right) \cdot \Xi_K \cdot \Xi_{lp} \cdot \Xi_f\right) dt$, which was coupled with flame wrinkling factors, Eqs. (4)-(6).

The flame wrinkling factor Ξ_f is calculated following "standard" model Eq.(6), i.e. as a function of flame distance from ignition point, based on the fact that this factor "kicks-in" at a later stage of combustion (beyond radius R_0), when flame size is already comparable to the flame displacement due to buoyancy.

3.3 Dependence of characteristic radius R_0 on mixture composition

The LES deflagration model so far contained the only adjustable coefficient ψ. Characteristic radius for the development of fully turbulent flame wrinkling regime R_0 was kept equal R_0=1.0-1.20 m as found in experimental observations by Gostintsev et al. [22] for near-stoichiometric hydrogen-air mixtures. However, the characteristic radius may change with mixture reactivity and a smaller experimentally observed value R_0=0.25 m was reported in the same publications [22] for more reactive stoichiometric hydrogen-oxygen mixture. In the presented simulations we made an assumption that for the thermo-diffusively unstable and more reactive lean hydrogen-air mixtures the onset of a fully turbulent flame propagation regime may occur earlier and the characteristic radius R_0 may be smaller. In turn, the radius R_0 will also directly affect the characteristic radius $R_{0_{lp}}$, characteristic times t and t_{0lp}, which all together will have a profound effect on the deflagration dynamics.

3.4 Burning velocity uncertainty

The other uncertainty the authors faced was choice of the burning velocity S_u. Closer to stoichiometric mixtures the LES model utilised burning velocity dependence on hydrogen concentration following experimental research [16]. However, in the area of small concentrations experimental data has large scatter and the burning velocity of 10% vol. hydrogen-air mixture varied from approximately 0.07 to 0.12 m/s for the same experimental setup.

Properties of 10% vol. hydrogen-air mixture relevant to combustion and LES deflagration modelling was used in simulations are summarised in Table 1.

Table 1. Properties of 10% hydrogen-air mixture.

Burning velocity S_u, m/s	0.074 m/s
Combustion products expansion coefficient E	3.52
Maximum flame wrinkling factor due to turbulence generated by flame front $\Xi_K^{\max}$	1.46
Maximum leading point flame wrinkling factor $\Xi_{lp}^{\max}$	2.34
Maximum fractals flame wrinkling factor Ξ_f for central ignition	1.15
Maximum fractals flame wrinkling factor Ξ_f for front and rear ignition	1.18

3.5 Calculation domain, boundary conditions and numerical details

The calculation domain was designed to accommodate the experimental enclosure and area around it for pressure wave propagation. For this the vented enclosure was located centrally inside of the hemispherical domain of 50 m radius. Based on the experimental paper [7] the enclosure sizes were 10×4.0×3.0 m, the centrally located vent size was 0.74×0.74 m (0.55 m^2 area). The enclosure was dipped inside of a shelter which was modelled as a void. The simulated vented enclosure and surrounding it shelter are shown in Fig. 1.

The calculation domain was meshed using tetrahedral control volumes (CV) with total number 267,869. No phenomena, which potentially could affect deflagration dynamics, were expected outside of the enclosure, and the finest mesh with characteristic CV size 0.15 m was used inside of the enclosure. Characteristic CV size immediately in front of the enclosure was equal 0.20 m and it was growing up to 5.0 m at the calculation domain boundary. Central cross section of the calculation domain and numerical mesh are given in Fig. 2 (a), and the enlargement of the vented enclosure is given in Fig. 2(b).

For all solid surfaces (ground, outer shelter surface, inner enclosure walls) there were implemented impermeable, non-slip, adiabatic boundary conditions. For the boundary with ambient atmosphere the non-reflective far-field pressure condition was used. Initial conditions were matching those in the experiment: initial temperature was equal to 293 K, ambient pressure equal to 101,325 Pa. Both the mixture and the ambient atmosphere were initially quiescent, u=0, u'=0. Hydrogen concentration inside of the vented enclosure was set to 10% vol.

ANSYS Fluent software was used as a platform for implementation of the LES deflagration model. Simulations were run using explicit solver, time-marching was modelled using Runge-Kutta scheme, 2nd order upwind scheme was used for convective terms, and 2nd order central-difference scheme for diffusion terms. To ensure stable simulations Courant-Friedrichs-Levy number was set to 0.8.

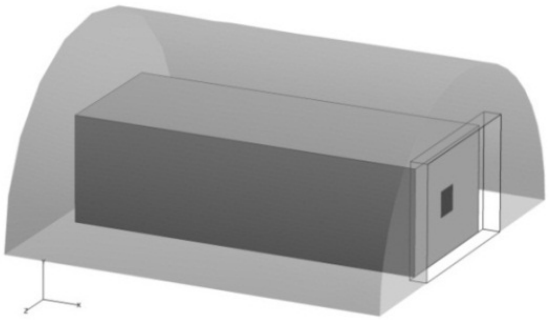

Figure 1. Combustion chamber and housing structure geometry.

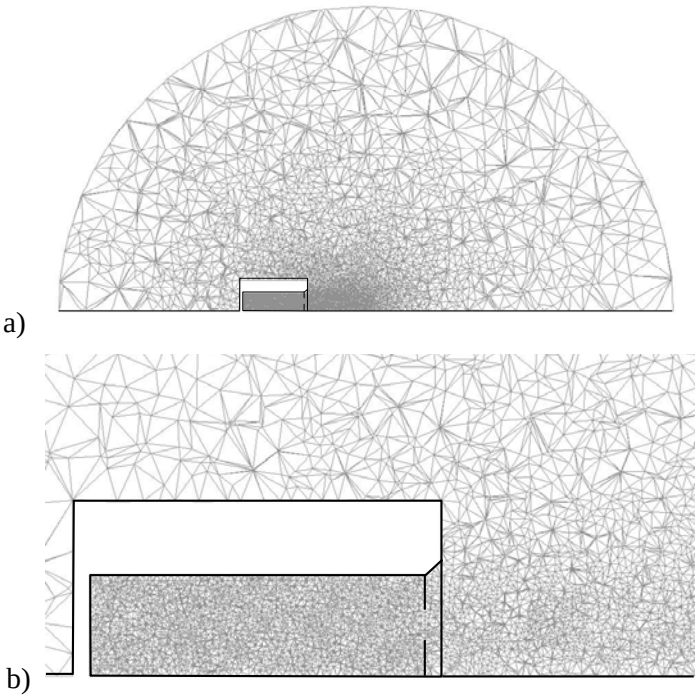

Figure 2. Numerical mesh: a) overall domain, b) combustion chamber

4.0 SIMULATION RESULTS FOR 10% H2-AIR DEFLAGRATION

4.1 Modelling of rear-wall ignition deflagration

In all simulations described below the initial value of burning velocity was equal to S_u=0.074 m/s, i.e. to its minimum value following study by Lamoureux et al. [16], and the fractal dimension was fixed to the theoretical value D=2.33. Preliminary simulations results showed that the characteristic radius for onset of fully turbulent flame propagation regime should be reduced to reproduce pressure dynamics at initial period and after initial simulations it was chosen as R_0=0.55 m. Coefficient ψ was equal to 1.0 that is characteristic for lean hydrogen-air mixtures [our previous paper]. In all simulated cases in this study the vent was opened as one piece, instantaneously. Experimental pressure dynamics was digitised based on the curves presented in the original experimental paper [7]. As exact ignition time was not known, all experimental pressure dynamics curves were set back in time to match simulation dynamics at initial combustion period in closed space before venting was initiated; the adjustment time shift was equal Δt=2.4 s for rear-wall, and Δt=2.75 s for central and front-wall ignitions respectively.

The simulation programme to investigate the impact of acoustic instability on combustion intensification for the rear-wall ignition case is listed in the Table 2. To match the experimental dynamics it was necessary to introduce the additional flame wrinkling factor. The factor was set to occur at the moment of vent opening (vent opening overpressure was equal Δp=3.8 kPa), which could generate a pressure wave giving rise to combustion intensification. Simulations demonstrated that vent opening usually happened when the buoyant flame touches and starts spread along the ceiling that as well could be a reason for initiation of acoustic waves within the enclosure. The ad-hoc wrinkling factor was a multiplier to the burning velocity S_u=0.074 m/s, the resulting value of "effective" burning velocity is shown in Table 2 in brackets. Here and in all following simulations the combustion acceleration was assigned to develop over period of 0.016 s, which is approximately the time of acoustic wave travelling through the enclosure length. It is worth noting that "effective" burning velocity is practically within the range of laminar burning velocity scatter 0.074-0.12 m/s measured in controlled tests [16].

Table 2. Simulation programme for rear-wall ignition.

Simulation	Ad-hoc wrinkling factor	Time of ad-hoc factor application
R1	1.35 (S_u=0.100 m/s)	t=1.37 s (vent opening)
R2	1.49 (S_u=0.110 m/s)	t=1.37 s (vent opening)
R3	1.62 (S_u=0.120 m/s)	t=1.37 s (vent opening)

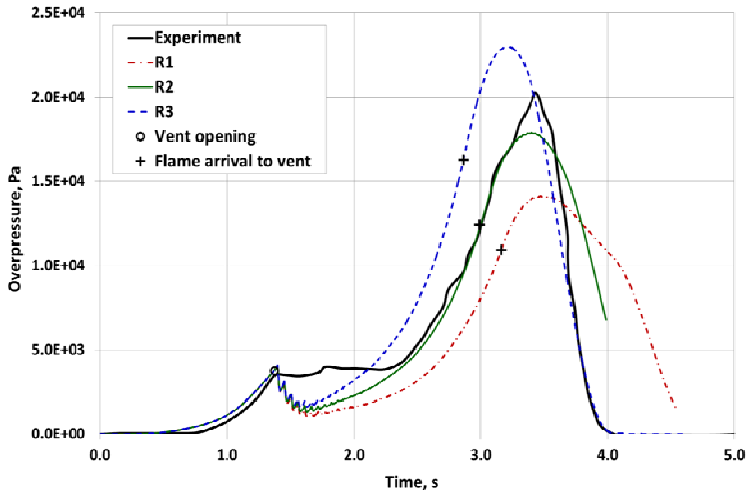

Figure 3. Comparison of experimental and simulated pressure dynamics for rear-wall ignition

The simulation results for rear-wall ignition are shown in Fig. 3. The agreement with the experimental pressure gradient in the largest pressure peak is achieved for the case R2 with ad-hoc wrinkling factor of 1.49. The best agreement for the overpressure would be between acceleration factors 1.49 (R2) and 1.62 (R3). The moment when combustion products start to be vented from the enclosure is indicated in Fig. 3 for all three cases by crosses. The combustion acceleration was set at t=1.37 s, i.e. long time before the flame appeared at the vent (t=2.86, 2.99 and 3.16 s for R1, R2 and R3 cases respectively). The simulated pressure dynamics has some "dip" after numerical opening of the vent at t=1.35 s not observed in the experimental curve, so development of real combustion intensification with time was more complex and soon after t=1.35 s it was even higher than simulated. Another possible explanation is opening of the vent in parts.

4.2 Modelling of central ignition deflagration

Combustion acceleration factors for modelling of central ignition are given in Table 3. The vent opening was modelled at overpressure Δp=2.8 kPa which occurred at t=1.16 s. Flame arrived to the vent at approximately t=2.30 s (marked by a cross). Additional acceleration factor kicked-in only after the combustion products started to vent into the ambient environment at t=2.55 s. Any earlier combustion acceleration would result in significant overprediction of overpressure during t=1.35-2.50 s (observed in preliminary simulations, not demonstrated here). The pressure dynamics obtained with different acceleration factors is shown in Fig. 4. The best overpressure was achieved with the acceleration factor 1.7, while the best pressure gradient on the rising branch of the second peak is achieved with the factor 1.8. There is also a similar to the rear-ignition case "dip" in simulated pressure dynamics after the vent opening at t=1.16 s not reproduced, suggesting that some combustion acceleration occurring after the vent opening was missed in simulations. Another discrepancy with experiment is absence of a peak at the very final stage of deflagration at $t\approx$3.75 s.

Table 3. Simulation programme for central ignition

Simulation	Ad-hoc wrinkling factor	Time of ad-hoc factor application
C1	1.0 (S_u=0.074 m/s)	t=2.55 s (products venting)
C2	1.5 (S_u=0.111m/s)	t=2.55 s (products venting)
C3	1.7 (S_u=0.126m/s)	t=2.55 s (products venting)
C4	1.8 (S_u=0.133 m/s)	*t=2.55 s (products venting)*

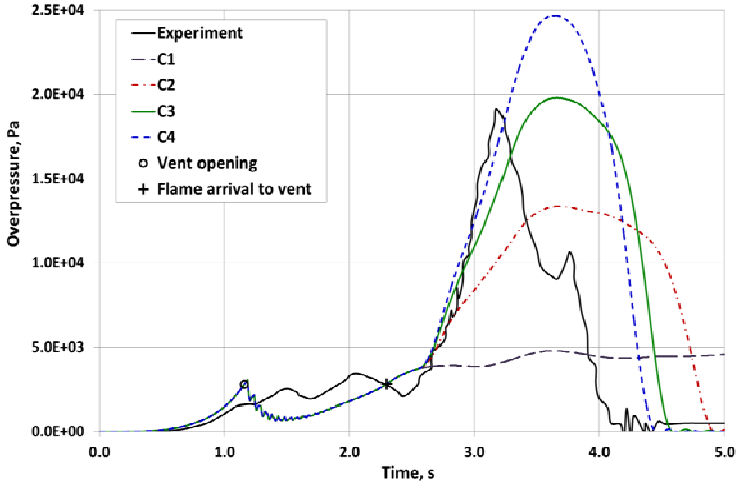

Figure 4. Comparison of experimental and simulation pressure dynamics for central ignition

4.3 Modelling of front-wall ignition deflagration

To reproduce the pressure dynamics for the front-wall ignition there was necessary to use two multipliers for the burning velocity (divide the application of the ad-hoc factor in two stages): one was invoked at the vent opening (opening overpressure Δp=3.8 kPa, t=1.03 s) and the second one was triggered at t=3.30 s. The major regularities here are the same as for the rear-wall and central ignition: vent opening practically coincided with the flame arrival to the ceiling (products venting in this case occurred immediately after that), “dipped” simulated pressure dynamics compare to the experiment after the vent opening. Final experimental peak occurred after the maximum one at $t\approx$5.2 s, is much more pronounced for the front-wall ignition, and, similar to the central ignition, not reproduced in simulations.

Table 4. Simulation programme for front-wall ignition

Simulation	Ad-hoc wrinkling factor	Time of ad-hoc factor application
F1	1.49 (S_u=0.11 m/s) 1.00 (S_u=0.11 m/s)	t=1.02 s (vent opening) t=3.30 s (flame venting)
F2	1.49 (S_u=0.11 m/s) 1.20 (S_u=0.132 m/s)	t=1.02 s (vent opening) t=3.30 s (flame venting)
F3	1.49 (S_u=0.110 m/s) 1.40 (S_u=0.154 m/s)	t=1.02 s (vent opening) t=3.30 s (flame venting)

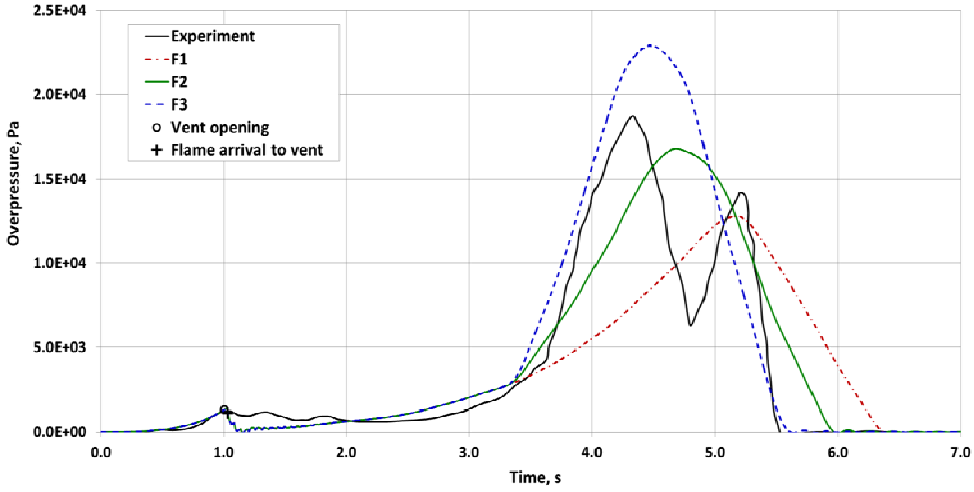

Figure 5. Comparison of experimental and simulation pressure dynamics for front-wall ignition

4.4 Discussion

The simulations demonstrated that in all studied cases additional to previous model wrinkling factor has to be applied to reproduce the dynamics of deflagration process. This factor is of the order of2 and increases from 1.62 for rear wall ignition to 1.8 for central ignition and reaches about 2.1 for the front-wall ignition respectively.

The difference in value of add-hoc wrinkling factor with location of ignition indicates that the nature of the factor origin is related to acoustic instability of combustion in this large-scale facility. The smallestvalue of the factor is for rear ignition when the pockets of unburned gas at the end of the process are minimum. Acoustic instability is in essence Rayleigh-Taylor instability that is repeatedly caused by travelling pressure wave.

In case of the central ignition the phenomenon responsible for combustion acceleration could be Rayleigh-Taylor instability caused by vented flow acceleration based on the suggestion by Solberg et al. [4]. Indeed, by t=2.55 s the flame filled a significant area under the enclosure ceiling, but was far from occupying most of the enclosure, when the acoustic oscillations could be expected. It is interesting that there was no need for combustion acceleration at the moment of vent opening.

For the front-wall ignition the combustion acceleration was the most complex. As the time of vent opening and combustion products venting practically coincided, the combustion acceleration could be a result of interference of both processes – rearfaction wave generated due to vent opening and flow acceleration due to venting. The second acceleration factor required for front-wall ignited case was very likely due to combustion-acoustic interaction at the later stage of combustion.

It is interesting that though the total value of combustion acceleration factor is up to 2.1 times, the increase of the burning velocity (from initial value S_u=0.074 to S_u=0.154 m/s in case F3) still close to the limits of the experimental data scatter for laminar burning velocity measured by different researchers, e.g. [23], and even by the same authors using the same experimental setup, see [16], where laminar burning velocity for the 10% mixture gave values about S_u=0.07 and 0.12 m/s.

Simulated pressure dynamics for all cases demonstrated a “dip” in pressure immediately after vent opening, while there was no such a “dip” in experimental records. The pressure wave generated during vent opening is relatively weak to cause appreciable pressure shocks. On the other hand, combustion acceleration should be substantial to maintain pressure at nearly the same level after the vent opening.

Combustion intensification, modelled using constant value acceleration factor, didn’t reproduce the final pressure peak following the maximum overpressure and observed for the central ignition at t≈3.75 s and for the front-wall ignition at t≈5.2 s. The authors believe that the final pressure peak appeared because combustion intensity at the final stage of deflagration was increasing with time due to known fact that acoustic instability is the most pronounced at the end of the process. The larger final pressure peak corresponding to the front-wall ignition should correspond to the larger quantity of unburned hydrogen and longer time available for developing of combustion acceleration. Additional simulations should clarify this hypothesis.

5.0 CONCLUSIONS

Pilot study of the LES deflagration model performance in application to lean hydrogen-air mixtures was performed using example of simulation of 10% vol. hydrogen deflagrations in a 120 m^3 enclosure with 0.55 m^2 vent area ignited at rear, centre, and at front wall.

Phenomena not accounted in the applied version of the LES deflagration model – flame instabilities, combustion-acoustic interaction, etc. – were modelled using a constant combustion acceleration coefficient. To match the maximum experimental overpressure the total acceleration coefficient value was as high as 2.1 (for near front wall ignition).

Simulation results seem to confirm that the mechanisms triggering combustion acceleration of lean hydrogen mixtures will depend on deflagration scenario. Deflagration with the front-wall ignition had the most complex dynamics of combustion acceleration. The simulated rear-wall ignited deflagration required the smallest additional flame acceleration and its venting didn’t cause significant contribution to combustion instabilities and combustion augmentation.

REFERENCE

1. Molkov, V., Fundamentals of Hydrogen Safety Engineering, BookBoon, 2012, ISBN 978-87-403-0226-4 (http://bookboon.com/en/textbooks/search?q=author%3A%22Vladimir%20Molkov%22).
2. Van Wingerden, C.J.M., and Zeeuwen, J.P. On the role of acoustically driven flame instabilities in vented gas explosions and their elimination, *Combustion and Flame*, **1**, No.1, 1983, pp. 109-11.

3. Cooper, M.G., Fairweather, M., and Tite, J.P, On the mechanisms of pressure generation in vented explosions, *Combustion and Flame*, **65**, 1985, pp.1-14.
4. Solberg, D.M., Pappas, J.A., and Skramstad, E. Experimental investigation on flame acceleration and pressure rise phenomena in large scale vented gas explosions . Third Int. Symp. Loss Prevent. and Safety Promot. Process Ind., Basel, **3**, 1980, pp.16/1295-16/1303.
5. Leyer, J.-C., and Manson, N. Development of vibratory flame propagation in short closed tubes and vessels. *13th Symposium (International) on Combustion*. Elsevier, 1971.
6. Bauwens, C.R., Chaffee, J., and Dorofeev S.B. Vented explosion overpressures from combustion of hydrogen and hydrocarbon mixtures, *Int. Journal of Hydrogen Energy*, **36**, 2011, pp.2329-2336.
7. Kumar, R.K., Vented Combustion of Hydrogen-Air Mixtures in a Large Rectangular Volume, Collection of technical papers - 44th AIAA Aerospace Sciences Meeting, **6**, 2006, pp.4398-4406.
8. Verbecke, F. Formation and combustion of non-uniform hydrogen-air mixtures, PhD Thesis, University of Ulster, 2009.
9. García, J., Baraldi, D., Gallego, et al. An intercomparison exercise on the capabilities of CFD models to reproduce a large-scale hydrogen deflagration in open atmosphere. *Int. Journal of Hydrogen Energy*, **35**, No.9, 2010, pp. 4435-4444.
10. Makarov, D., Verbecke, F., Molkov, V., et al. An intercomparison of CFD models to predict lean and non-uniform hydrogen mixture explosions. *Int. Journal of Hydrogen Energy*, **35**, No.11, 2010, pp. 5754-5762.
11. Baraldi, D, Kotchourko, A., Lelyakin, A., et al. An inter-comparison exercise on CFD model capabilities to simulate hydrogen deflagrations with pressure relief vents, *Int. Journal of Hydrogen Energy*, **35**, No.22, 2010, pp. 12381-12390.
12. Baraldi, D., Kotchourko, A., Lelyakin, A., et al. An inter-comparison exercise on CFD model capabilities to simulate hydrogen deflagrations in a tunnel, *Int. Journal of Hydrogen Energy*, **34**, No.18, 2009, pp.7862-7872.
13. Makarov, D., Verbecke, F., Molkov, V., et al., An inter-comparison exercise on CFD model capabilities to predict a hydrogen explosion in a simulated vehicle refuelling environment, Int. Journal of Hydrogen Energy, **34**, No.6, pp. 2800-2814.
14. Yakhot, V., and Orszag, S.A., Renormalization group analysis of turbulence. I. Basic theory, *Journal of Scientific Computing*, **1**, No.1, 1986, pp.3–51.
15. Yakhot, V., Propagation Velocity of Premixed Turbulent Flames, *Combustion Science and Technology*, **60**, 1988, pp.191-214.
16. Lamoureux, N., Djebaili-Chaumeix, N., and Paillard, C. E., Laminar flame velocity determination for H2-air-steam mixtures using the spherical bomb method, *Journal de Physique de France IV*, **12**, 2002, pp. 445–452.
17. Babkin, V. S., Private communication. Institute of Chemical Kinetics and Combustion, Siberian Branch, Russian Academy of Science, Novosibirsk, 2003, Russia.
18. Karlovitz, B., Denniston, D.W.Jr., and Wells, F.E., Investigation of Turbulent Flames, *The Journal of Chemical Physics*, **19**, No.5, 1951, pp. 541-547.
19. North, G.L., and Santavicca, D.A., The fractal nature of premixed turbulent flames, *Combustion Science and Technology*, **72**, 1990, pp.215-232.
20. Zimont, V.L., and Lipatnikov, A.N., A numerical model of premixed turbulent combustion of gases, *Chemical Physics Reports*, **14**, No.7, 1995, pp. 993-1025.
21. Molkov, V.V., Nekrasov, V.P., Baratov, A.N., and Lesnyak, S.A., *Combustion, Explosions and Shock Waves*, **20**, 1984, pp.149-153.
22. Gostintsev, Yu.A., Istratov, A.G., and Shulenin, Yu.V. , Self-similar propagation of a free turbulent flame in mixed gas mixtures, *Combustion, Explosion and Shock Waves*, **24**, No.5, 1988, pp.63-70.
23. Dahoe A., Laminar burning velocities of hydrogen–air mixtures from closed vessel gas explosions, *Journal of Loss Prevention in the Process Industries*, **18**, 2005, pp.152-166.